Design of omnidirectional and multiple channeled filters using one-dimensional photonic crystals containing a defect layer with a negative refractive index

Kun-yuan Xu, Xiguang Zheng,* Cai-lian Li, and Wei-long She
State Key Laboratory of Optoelectronic Materials and Technologies, Institute of Laser and Spectroscopy, Sun Yat-sen (Zhongshan) University, Guangzhou 510275, China

(Received 12 August 2004; revised manuscript received 24 March 2005; published 13 June 2005)

The band structures of one-dimensional photonic crystals containing a defect layer with a negative refractive index are studied, showing that the defect modes possess three types of dispersion: positive, zero, and negative types. Based on these three types of dispersion, practical designs for large incident angle filters without polarization effect and for narrow frequency and sharp angular filters are suggested. Moreover, the splitting of one degenerate defect mode into multiple defect modes is observed in the band gap when the parameters of the defect layer vary. This mode splitting phenomenon can be used to design multiple channeled filters or filters with a rectangular profile. The dispersion multiplicity of the defect modes can be understood by an approximate formula, and the critical condition for the defect mode splitting is also analyzed. Based on these analyses, practical optimization design of omnidirectional filter is also suggested.

DOI: 10.1103/PhysRevE.71.066604 PACS number(s): 42.70.Qs, 41.20.Jb, 42.79.−e

I. INTRODUCTION

Photonic crystals (PCs) have attracted much scientific interest during the past decade due to their novel electromagnetic properties and potential applications [1,2]. It has been proved that the inference of Bragg scattering in a periodical dielectric structure is the reason to form a photonic band gap (PBG). When the periodicity is broken by introducing a defect into a PC, a localized defect mode will appear inside the Bragg gap due to change of the interference behavior of light. In the case of the conventional one-dimensional (1D) PCs, which are made of dielectric media with positive refractive indices (also called right-handed material), it is well known that, as the incident light changes from normal to oblique incidence, the effective optical lengths of all the medium layers, including the defect layer, reduce. This strongly influences the interference process within the PCs, and then causes both the Bragg gap and the defect modes to shift into higher frequencies. For this reason, the phenomenon of PBG has been used for mirrors only under a narrow range of frequencies of light incident at a particular angle or within a particular angular range; and that of the defect modes has been used for filters also only under the limit to the normal incidence.

Thus, how to overcome these angular effects have attracted great interest recently. Based on the mechanism of Bragg scattering, Fink *et al.* [3,4] realized a dielectric omnidirectional reflector. On the other hand, some researchers attempted to realize a PBG related to the mechanism beyond Bragg scattering [5,6] in the left-handed materials (LHM). Such materials possess negative refractive indices ($n = \sqrt{\varepsilon}\sqrt{\mu}$), which is due to simultaneously negative permeability and permittivity [7,8]. It has been demonstrated that stacking alternating layers of positive and negative media leads to a type of PBG corresponding to a zero (volume) averaged refractive index [5]. Further investigations showed that such zero-averaged refractive index could result in an omnidirectional gap, and that the defect modes in zero-$\bar{n}$ gap were weakly dependent on the incident angles [6].

It is worthy of notice that the mechanism of Bragg scattering also works in some cases of 1D PCs containing LHM [9], and can result some particular phenomena, such as unusual narrow transmission bands [10], which are expected to be forbidden regime in the case of conventional 1D PCs. In this work, we study the properties of the defect modes in 1D PCs containing a defect layer with a negative refractive index, and demonstrate that the defect modes possess many unique properties, such as dispersion multiplicity, splitting of degenerate modes, and transmission independence on the incident angles, which can also be explained by the mechanism of Bragg scattering. The present paper is organized as follows. In Sec. II, the dispersion relation of the defect modes is studied numerically, and three (positive, zero, and negative) types of dispersion of the defect modes are demonstrated. Applications of the dispersion multiplicity are also suggested. Then in Sec. III based on Bragg scattering, a formula is deduced for understanding the dispersion multiplicity of defect modes. In Sec. IV, the splitting of one degenerate defect mode into multiple defect modes in the band gap is investigated, and the critical condition for this mode splitting transition is analyzed. The practical design for filters with a rectangular profile and multiple channeled filters based on the splitting transition of defect modes is suggested. Moreover, distribution of the electronic fields in the 1D PCs is calculated. Efforts are focused on optimization design for omnidirectional filters in Sec. V. Three types of criteria for zero dispersion are proposed. Optimized parameters for the omnidirectional filters, according to the different criteria, are given by utilizing the formulas deduced in Secs. III and IV. We summarize our work in Sec. VI.

*Author to whom correspondence should be addressed. Electronic address: stszheng@zsu.edu.cn

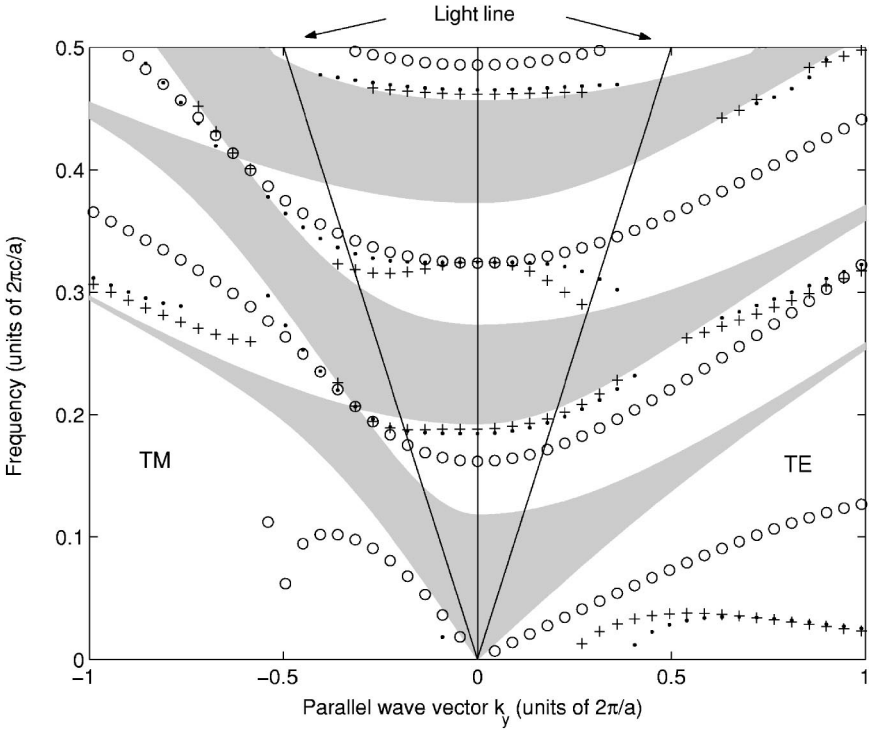

FIG. 1. Dispersion relationships of the defect modes in a PC containing a LHM defect layer. The parameters for the PC are $n_A=4.6$ and $n_B=1.6$ with a thickness ratio of $d_A/d_B=1.2/1.2$. The crossed, square and circled curves in the band gaps represent the defect modes corresponding to the different defect layers with $n_C=-1.6$, -1.95, and -3.6, respectively. The optical thickness of the defect layer in any case is one half of the optical thickness of a PC cell. Three dispersion types (positive, zero, and negative dispersion) of the defect modes can be observed in the second band gap.

II. DISPERSION RELATION OF DEFECT MODES

We first choose a 1D PC which satisfies the necessary and sufficient criterion for omnidirectional reflectivity at a given frequency [3], then break the periodicity by introducing a defect layer with a negative refractive index into the PC to compose a system with the form of $(AB)^S ACA(BA)^S$, where A (B) represents a layer with a positive refractive index of n_A (n_B), a unitary permeability of μ_A (μ_B), and a geometrical thickness of d_A (d_B), and C represents a defect layer with a negative refractive index of n_C, a negative unitary permeability of μ_C, and a geometrical thickness of d_C. S is the periodic number of the subsystems, (AB) and (BA), and for an infinite system, $S\rightarrow\infty$. For the sake of simplification and with no influences upon our results, we assume that all the refractive indices are frequency independent. Let a wave be incident at an angle θ from vacuum onto the considered system. Suppose the incident wave has a wave vector $\vec{k}=k_x\hat{e}_x+k_y\hat{e}_y$ and a frequency of $\omega=c|\vec{k}|$, where c is the speed of light in vacuum, and $\hat{e}_x$ and $\hat{e}_y$ are the unit vectors along the x and y directions, respectively. The dispersion relation $\omega(K,k_y)$ of a perfect 1D PC has been given by Fink *et al.* [3] as follows:

$$K=\frac{i}{a}\ln\left(\frac{1}{2}\mathrm{Tr}(U^{(\alpha)})\pm\left\{\frac{1}{4}[\mathrm{Tr}(U^{(\alpha)})]^2-1\right\}^{1/2}\right), \qquad (1)$$

where $U^{(\alpha)}$ is a unitary 2×2 translation matrix relating the amplitudes of the forward and backward plane waves in a particular layer α of one cell in a layer to the amplitudes of the waves in the same layer of the adjacent cell, $a=d_A+d_B$ is the length of a period, and K is the Bloch wave number. The real or imaginary Bloch wave number corresponds to the propagating or the evanescent wave, respectively. The solution of Eq. (1) defines the band structure for the perfect 1D PC. When a defect is introduced, we have the additional real Bloch wave numbers in the band gaps, which read

$$K_D=\frac{i}{a}\ln\frac{Q\pm(Q^2+1)^{1/2}}{\mathrm{Tr}(U^{(\beta)})}, \qquad (2)$$

where

$$Q=\mathrm{Tr}(U^{(\alpha)}U^{(\beta)})-\frac{1}{2}\mathrm{Tr}(U^{(\alpha)})\mathrm{Tr}(U^{(\beta)}), \qquad (3)$$

and $U^{(\beta)}$, similar to $U^{(\alpha)}$, describes the relation between the amplitudes of the waves in the defect cell and its adjacent cell. The solution of Eq. (2) yields the dispersion relation of the defect modes.

In Fig. 1 are shown the projected band structures of the considered system. The corresponding parameters for the PC are $n_A=4.6$ and $n_B=1.6$ with a layer thickness ratio of $d_A/d_B=1.2/1.2$. The gray and white regions in Fig. 1 represent the pass and forbidden bands, respectively. The two oblique solid lines are so-called light lines [3] corresponding to the incidence with an angle of 90°. Between the light lines, all the incident angles are less than 90°. The crossed, square, and circled curves in the band gaps denote the defect modes corresponding to different defect layers with $n_C=-1.6$, -1.95, and -3.6, respectively. In all cases, the optical thickness of the defect layer is one half of the optical thickness of a single PC cell. According to the symbolic curves shown in Fig. 1, we know that the dispersion relations of the defect modes can change from negative to positive types with an increase of the absolute value of n_C. When a proper mediate value of n_C is chosen, e.g., $n_C=-1.95$ in our case, zero-dispersion emerges in a large range of k_y. This means that the frequencies of the defect mode are independent of the incident angles in a large angular range. It is well known that the

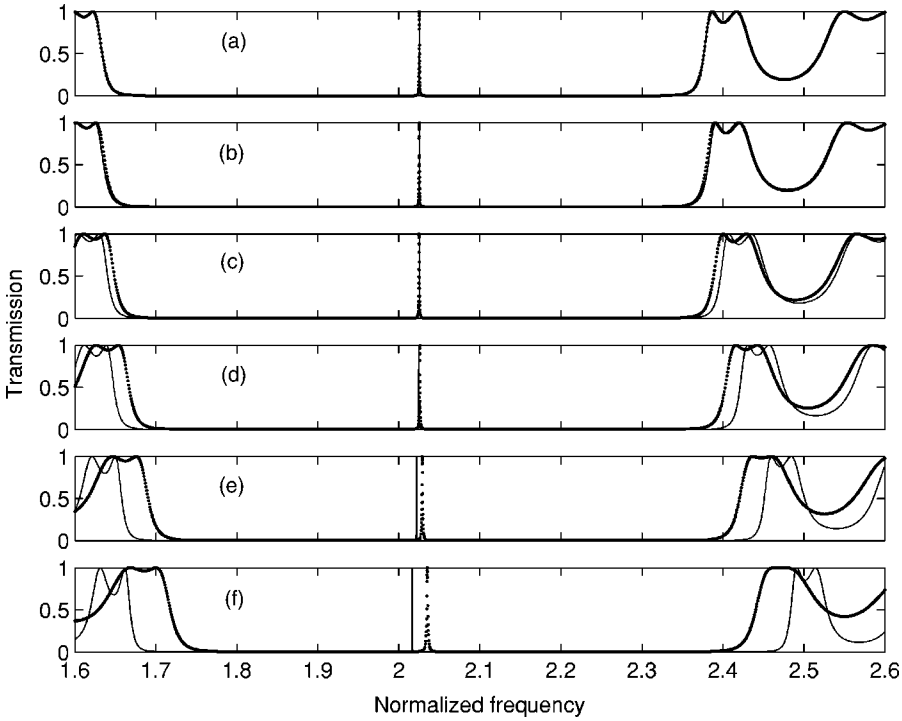

FIG. 2. Transmission spectra of a large incident angle filer with a structure form of $(AB)^6ACA(BA)^6$ at different incident angles. The filter is assumed to be placed in the air, and the parameters are the same as in Fig. 1 except for $n_C=-2.34$. From (a) to (f) are corresponding to the incident angles from 0° to 50°, respectively, with an interval of 10°. The solid and dot curves represent TE and TM modes, respectively.

dispersion relations of the defect modes in a conventional 1D PC are positive. And near zero dispersion of defect modes have been found in zero-$\bar{n}$ gaps recently [6]. But the negative dispersion of the defect modes is the additional phenomenon in our considered system. This new phenomenon comes from the physical property, a negative refractive index, of the defect layer. One knows, according to Snell's law, the refraction angle of negative index materials is negative. Then considering the requirements of the boundary condition of electric vectors, one has $k_z<0$. This means that the optical thickness of negative refractive index materials is negative. So, with the increase of the incidence angle, the optical thickness of the whole system will not always increase like that in conventional cases. When it decreases, the negative dispersion emerges (see Sec. III for more detailed mathematical explanations).

The zero-dispersion phenomenon is useful in designing large incident angle, and even omnidirectional, filters. In Fig. 2 are shown the transmission properties of a practical design for a large incident angle filer with a form of $(AB)^6ACA(BA)^6$. The transmission spectra are calculated by a transfer matrix method [11], and are respectively corresponding to the incident angles from 0° to 50° with an interval of 10°. The solid and dot curves correspond to TE and TM modes, respectively. The filter is assumed to be placed in the air, and all the parameters are the same as former except for $n_C=-2.34$. And we also assume that the optical thickness of one cell is a half of the reference wavelength $[\lambda_0=2\times(n_ad_a+n_bd_b)]$. Here, we choose $2\pi c/\lambda_0$ as the unit of frequency, called normalized frequency which is usually used in thin film optics, in Fig. 2. So the frequency range considered in Fig. 2 corresponds to that of the second forbidden gap in Fig. 1. With the value −1.95 of n_C in the present case, the dispersion of the defect modes is of zero type. The value of n_C for zero dispersion of the defect modes in this case is different from that in Fig. 1 because a finite structure is considered in this case while an infinite structure is considered in the case of Fig. 1. According to the transmission spectra shown in Fig. 2, we can see that the filter has neither angular nor polarizing effect when the incident angle is less than 30°, meaning zero dispersion of the defect mode within this incident angle. When the incident angle increases, TM mode shifts toward higher frequencies corresponding with positive dispersion, while TE mode shifts toward lower frequencies corresponding with negative dispersion.

Recently, Liang *et al.* [12] have proposed a technique to obtain narrow frequency and sharp angular defect mode in 1D PCs by combining two 1D defective PCs, which is useful in design for novel filters with both narrow-frequency passband filtering and sharp angular spatial filtering. The key of their technique is to design the two sub-PCs first to make the frequencies of the defect modes the same in the sub-PCs at a certain angle, and secondly to make the dispersion deviation of the defect modes as large as possible between the sub-PCs. The first requirement can be easily fulfilled by applying the scaling law [13]. In order to satisfy the second requirement, heterostructures were considered in their investigation. Here, because the defect modes with negative and positive dispersion can simultaneously emerge in 1D PCs containing a LHM defect layer, it is easy to design the same filters with homostructures of the sub-PCs. We consider a practical design for a such filer with a form of $(AB)^{S_1}AC_1A(BA)^{S_1}B(AB)^{S_2}A\alpha C_2A(BA)^{S_2}$, where α is a modulating parameter which determines the optical length of the defect layer C_2 and guarantees the same frequencies of the defect modes in the two sub-PCs at the incident angle of zero, and S_1 (S_2) is the number of the periods. The parameters for this structure are $n_{C1}=-1.6$, $n_{C2}=-3.6$, $\alpha=1.03131$, $S_1=4$, and $S_2=5$, and the other parameters are the same as former. In Fig. 3 are shown the frequency and inci-

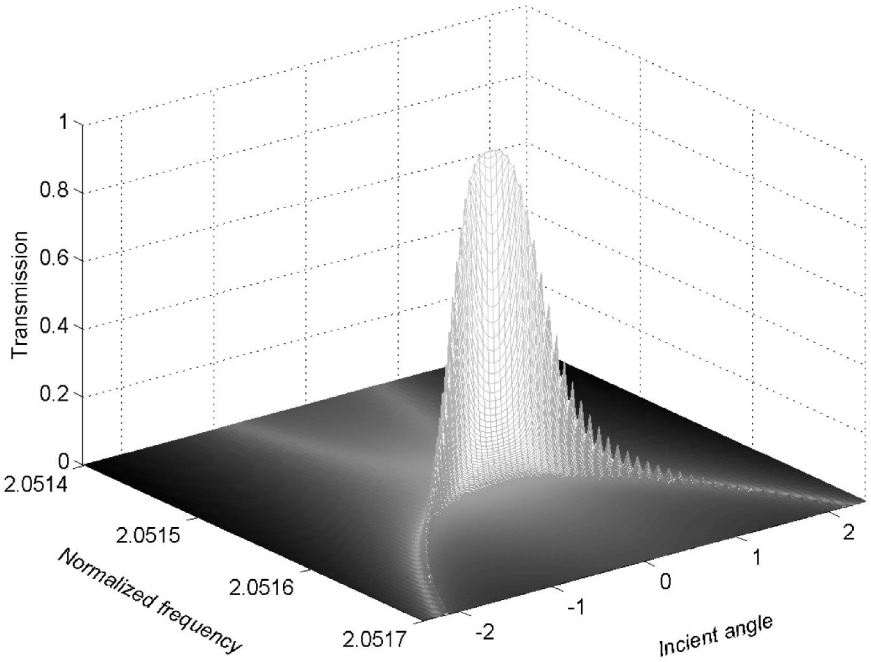

FIG. 3. Frequency and incident angle dependent transmission of a heterostructure with a structure of $(AB)^4AC_1A(BA)^4B(AB)^5A\alpha C_2A(BA)^5$. The refractive indices of layers C_1 and C_2 are −1.6 and −3.6, respectively, and $\alpha=1.03131$. The parameters of layers A and B are the same as in Fig. 2. The negative and positive incident angles are corresponding to TM and TE modes, respectively.

dent angle dependent transmission properties of the structure as described above. As shown in Fig. 3, negative and positive incident angles are corresponding to TM and TE modes, respectively. The frequency range of omnidirectional reflection is calculated to be $1.86\omega_0-2.32\omega_0$. It is also found that only the light within a narrow frequency pass-band $(2.0516\omega_0\pm0.0005\omega_0)$ and within a sharp breadth of the incident angles $(0°\pm2°)$ is allowed to be transmitted through the filter. Moreover, the negative dispersion of the defect mode in one of the sub-PCs is strongly suppressed, and the dispersion of the combined defect mode shows positive dispersion. The suppression of the negative dispersion comes from $S_1<S_2$. If $S_1>S_2$, the positive dispersion would be suppressed, and the combined mode would show negative dispersion. The situation of $S_1=S_2$ should be avoided, for the strong interaction of the defect modes with negative and positive dispersion would enlarge the frequency pass-band.

III. APPROXIMATE ANALYSIS OF DISPERSION MULTIPLICITY OF DEFECT MODES

In the previous section, we have numerically demonstrated the properties of the defect modes in 1D PCs containing a defect layer with a negative refractive index. Having an approximate analytical formula, one may more easily understand these unique properties such as dispersion multiplicity of the defect modes. For this reason, we perform an approximate analysis of the defect modes on the base of Bragg scattering mechanism. We now assume that the optical thicknesses of A, B and C, respectively, are $\lambda_0/4$, $\lambda_0/4$, and $g\lambda_0$ at a frequency of ω_0, where λ_0 is the wavelength corresponding to ω_0, and g is related to the properties of the defect layer. Therefore, the phase change between the forward and backward waves in the defect layer is

$$\theta(\omega,\phi)=-2\varepsilon(\omega,\phi)+\frac{4g\pi\omega\cos\phi}{\omega_0}, \tag{4}$$

where ε is the phase change resulted from Bloch scattering, and ϕ is the refractive angle in the defect layer. According to Smith's discussions [14], we know that the defect modes appear when θ is equal to $\theta_0=2N\pi(N=1,2,\ldots)$. Suppose $\theta_0=2\pi$ when $\omega=\omega_0$ and $\phi=0$. Thus, at the frequency of ω_0, one has

$$\Delta\theta(\phi)=\theta(\phi)-\theta_0=-2[\varepsilon(\omega_0,\phi)-\varepsilon(\omega_0,0)]+4g\pi(\cos\phi-1). \tag{5}$$

Pidgeon and Smith [15] have obtained the dependence of ε upon ϕ_e in the limit $n_r^S>15$, where $n_r=n_A/n_B$ and ϕ_e is the incidence angle. Substituting their results into Eq. (5) and assuming that ϕ_e is small enough, we have

$$\Delta\theta(\phi_e)=-\left(2J+\frac{2g\pi}{n_C^2}\right)\sin^2\phi_e, \tag{6}$$

where

$$J=\frac{1}{2}\frac{n_C\pi}{\mu_C n_A}\left[\frac{1}{n_A^2}\left(\frac{n_r^2}{n_r^2-1}\right)+\frac{1}{n_B^2}\left(\frac{n_r}{n_r^2-1}\right)\right],$$

which is always positive. The first term on the right-hand side of Eq. (6) represents the angular effect of the Bragg scattering in the 1D PC (called ABC effect), and the second term represents the angular effect due to the physical properties of the defect layer (called AD effect). According to Eq. (6), one can see that the ABC effect tends to push the defect modes into higher frequencies, while the AD effect tends to do the same thing or the opposite thing corresponding to whether the refractive index is positive or negative. If the value of g is determined, the increment of $|n_C|$ enhances the ABC effect and weakens the AD effect. In the case of a

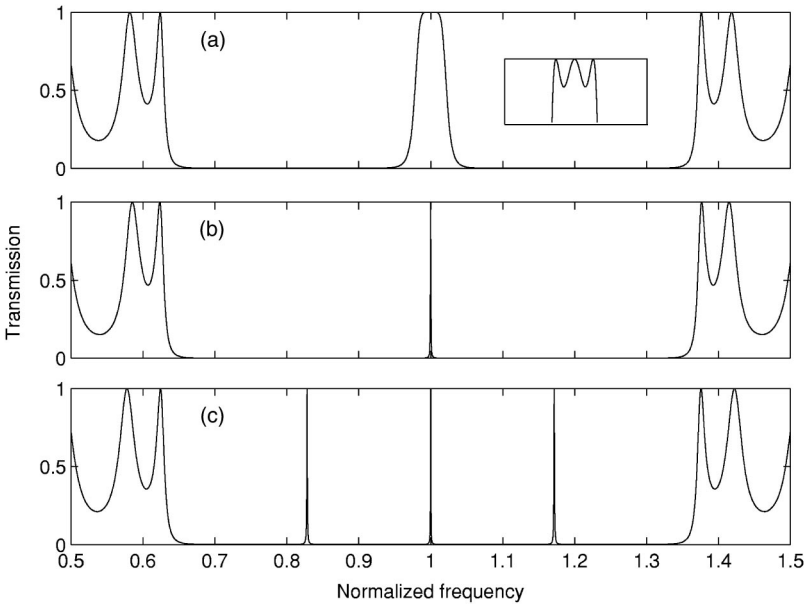

FIG. 4. Transmission spectra of the defect modes in the structure of $(AB)^4ACA(BA)^4$ at different refractive indices of the defect layer. The refractive indices of the layers A and B are $n_A=4.6$ and $n_B=1.6$. The optical thickness of layers A, B, and C are assumed to be $\lambda_0/4$, $\lambda_0/4$, and $-\lambda_0/2$, respectively. (a) Case of $n_C=-3$. The inset shows the spectral profile of the defect mode zoomed in on the top. (b) Case of $n_C=-3.2$; (c) case of $n_C=-2.8$.

defect layer with a positive refractive index, both effects contribute to increasing of the frequencies of the defect modes, and the dispersion of the defect modes is always positive. On the contrary, if the refractive index of the defect layer is negative, the two effects compete with each other. When the ABC effect is dominant, i.e., $[2J+2g\pi/n_C^2]>0$, the dispersion of the defect modes is positive. On the other hand, when the AD effect is dominant ($[2J+2g\pi/n_C^2]<0$), the dispersion is negative. And the zero-dispersion emerges when the two effects are balanced ($[2J+2g\pi/n_C^2]=0$).

IV. SPLITTING OF DEFECT MODES

According to the analysis as described in Sec. III, one can easily expect that there would be defect modes with a weak dependence on frequencies. In order to investigate this, we deduce the dependence of $\Delta\theta$ upon frequencies as follows:

$$\Delta\theta(\omega)=\theta(\omega)-\theta_0=-2\varepsilon(\omega)+\frac{4g\pi(\omega-\omega_0)}{\omega_0}. \qquad (7)$$

Utilizing Eq. (10A) in Ref. [15], and assuming that ω is sufficiently close to ω_0, we obtain

$$\Delta\theta(\omega)=-2\frac{\omega-\omega_0}{\omega_0}(t+2g)\pi, \qquad (8)$$

where $t=n_C/\mu_C n_B(n_r-1)$. Equation (8) indicates that the defect modes are frequency independent around ω_0.

Numerical simulations of the transmission spectra, as depicted in Fig. 4, are performed for the structure of $(AB)^SACA(BA)^S$, confirming the anticipation of Eq. (8). The parameters corresponding to Fig. 4(a) are $n_A=4.6$, $n_B=1.6$, $n_C=-3$, $g=-0.5$, and $S=4$, and other parameters are the same as those used in the approximate formulas; in this case, $t=-2g$. As shown in Fig. 4(a), the profile of the transmission spectrum of the defect modes exhibits an altiplano shape. In fact, if the spectrum is zoomed in on the top, one can see that the spectrum includes three vicinal defect modes [see the inset of Fig. 4(a)]. Further investigations show that, when $|n_C|$ increases, the two side modes move to the central mode and then the three modes superpose one another [see Fig. 4(b)]; contrarily, when $|n_C|$ decreases, the left mode shifts toward lower frequencies, and the right one shifts toward higher frequencies, while the central one remains immovable [see Fig. 4(c)].

The explanation of these transition phenomena is similar to that of the angular effects. Here, the critical condition of the transition is $t=-2g$. When $t>-2g$ (i.e., $|n_C|>3$), the frequency effect of Bragg scattering is dominant. In this case, the behaviors of the defect modes are similar to that in a conventional system; only a degenerate defect mode exists in the band gap. On the other hand, when $t<-2g$ (i.e., $|n_C|<3$), the frequency effect due to the physical properties of the defect modes is dominant, and the behaviors of the defect modes are unusual. In this case, the defect modes are nondegenerate, and multiple defect modes emerge in the band gap at different frequencies simultaneously.

The effect at the critical condition may be useful in design for novel filters with a rectangular profile, which could not be realized by only one conventional defect layer (usually by two). According to the above discussions, we know that the frequencies of the multiple defect modes and the frequency intervals between them can be respectively modulated by the optical length and the refractive index of the defect layer. In addition, half-widths of the defect mode can also be reduced by increasing the value of S. Considering all of these factors, we believe that the phenomena of emergence and splitting of multiple defect modes in 1D PCs containing defect layers of LHM can be used to design multiple channeled filters [as an example, see Fig. 4(c)], which is difficult to realize by conventional dielectric structures [16].

In the case of the conventional PCs, it is well known that a defect mode is usually localized since strong field localization emerges inside the defect at the corresponding frequency [13]. It is also known that many possible applications in optical devices are based on field localizations [17]. Thus, it is worth of studying the field distribution inside the PCs

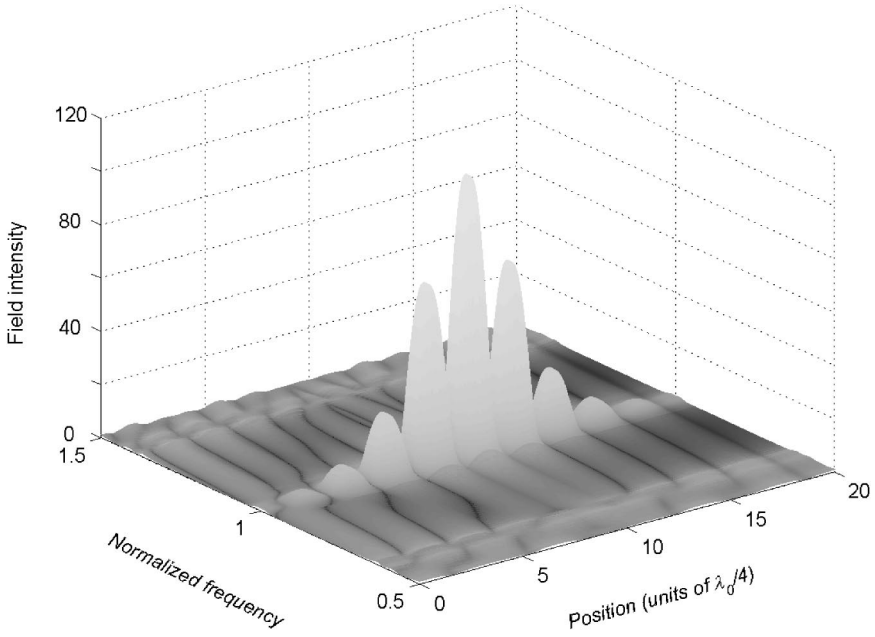

FIG. 5. Field distributions in 1D defective PCs corresponding to Fig. 4(a).

containing materials of negative index. In Figs. 5 and 6 are shown the numerical simulations of the field distributions, which are corresponding to Figs. 4(a) and 4(c), respectively. The calculation scheme is derived from a transfer matrix method [18]. As shown in Figs. 5 and 6, strong localizations can be found in the dielectric structures at the frequencies of the defect modes; the defect mode of altiplano shape shown in Fig. 4(a) results a localized band. Moreover, if the spectra in Fig. 6 is zoomed in on a frequency range between two neighboring strong localized bands, for example, a range from $1.01\omega_0$ to $1.16\omega_0$, week localization can be found in the defect layer (see Fig. 7). As a comparison, the field distribution in a conventional PC with the same absolute values of the structure parameters as used for Figs. 6 and 7 is also calculated and depicted in Fig. 8. As shown in Fig. 8, in the case of the conventional PC, electromagnetic fields in the dielectric structure exhibit more evanescent and less localized characteristics. We contribute the physical reason of these different characteristics to the fact that photons may tunnel through a much greater distance in the structure containing an LHM layer with the same absolutes value of refractive index and relative permeability and the same thickness as in the conventional structure in which only right-handed materials are included [19].

V. OPTIMAL DESIGN FOR OMNIDIRECTIONAL FILTERS

It is known that the optical properties of conventional thin film filters are relevant to incidence angle and polarization of the incident light [20], even those based on the defect modes in omnidirectional gaps [11,21]. So they are usually used under the limit of the normal incidence. To those of non-

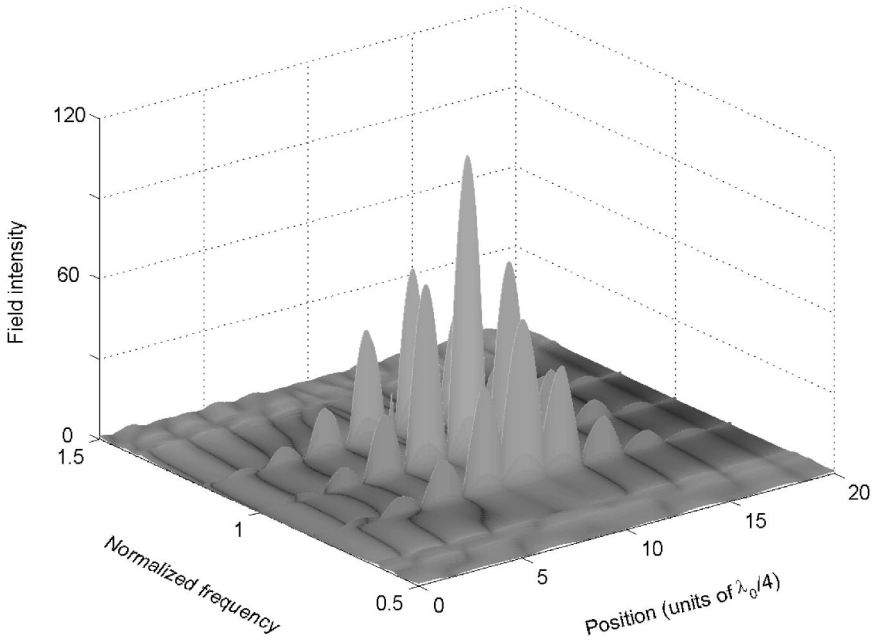

FIG. 6. Field distributions in 1D defective PCs corresponding to Fig. 4(c).

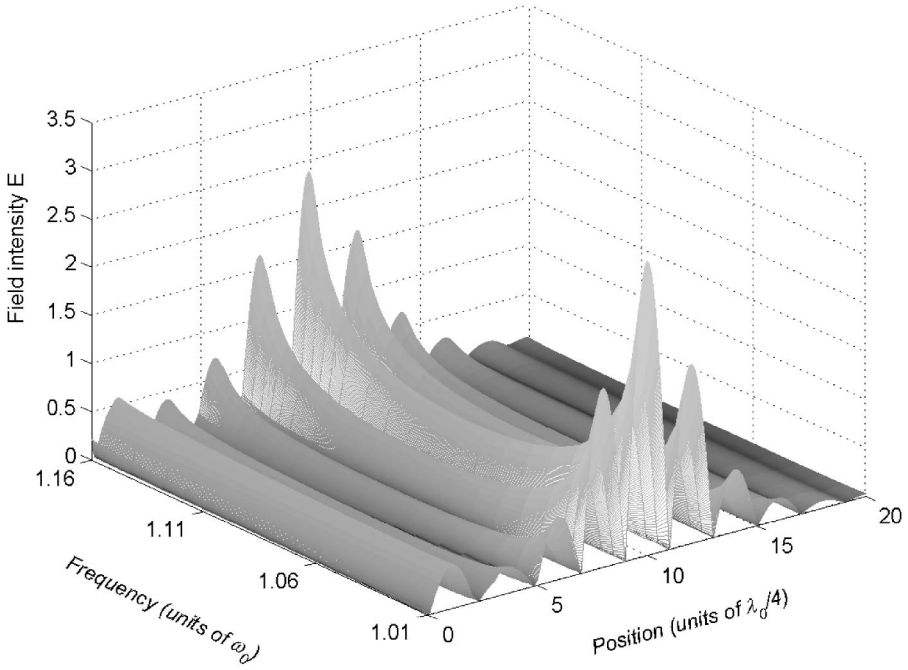

FIG. 7. Field distributions in the frequency range from $1.01\omega_0$ to $1.16\omega_0$ between two neighboring strong localized bands in Fig. 6. Week localization of the fields can be observed in the defect layer.

normal incidence, much effort has been put on them [22–24], but only for one special incidence. The use of such types of filters is in the case of collimated light. But in other cases, for example in the case of the scattering light or seriously focused light (such as filters being placed very near the focal plane), large incidence angle or omnidirectional filters may be suitable.

Analyses in Secs. III and IV provide a clue to optimal design for omnidirectional filters.

It is important to determine a suitable range of the structural parameters before any optimal design is performed. Equations (6) and (8) in Secs. III and IV are useful in seeking a correct range of the structural parameters for an optimized omnidirectional filter.

With both left-hand sides of Eqs. (6) and (8) equal to zero, we can calculate the relations between n_C and n_B in the two critical conditions, and depict two critical curves, respectively labeled curves *a* and *b*, as shown in Fig. 9. These two curves cross at $n_B=1.76$. According to discussions in Sec. IV, we know that there will exist multiple nondegenerate defects in the forbidden gap if the structural parameters are chosen in the region below curve *b* in Fig. 9. So, this region is not suitable for an omnidirectional (or large angle) filter, even though the dispersion of the defect mode is of zero type. Meanwhile, discussions in Sec. III imply that zero-dispersion phenomenon emerges when the structural parameters are chosen around about curve *a* in Fig. 9. Therefore, the suitable range of the structural parameters for an omnidirectional

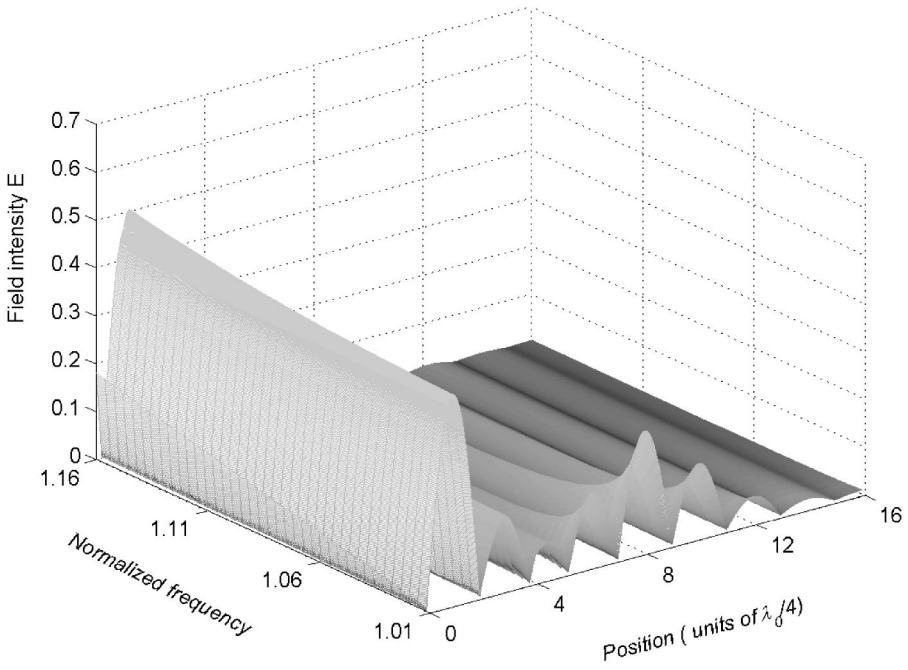

FIG. 8. Field distributions in a conventional PC.

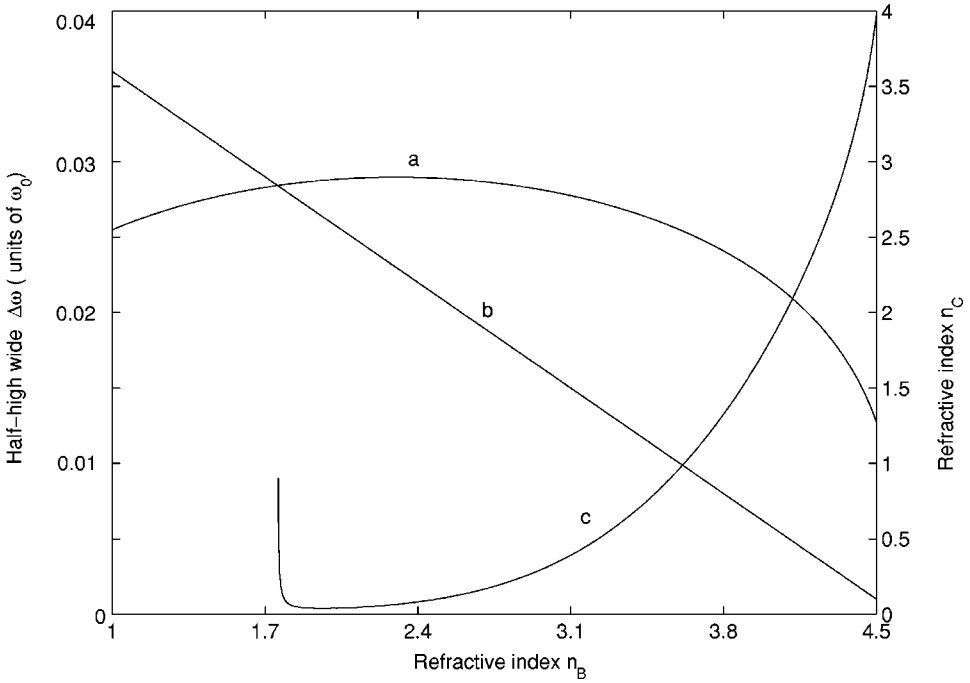

FIG. 9. Critical curves for dispersion multiplicity (a) and mode splitting of the defect modes (b). Curve *c* shows the FWHM of the defect mode transmission bands with the structural parameters corresponding to curve *a* when the incidence of plane wave is normal.

filter is within the region above curve *b* and at the same time round curve *a* as well. This also implies that n_B should be larger than 1.76.

Choosing the structural parameters corresponding to curve *a*, we can calculate the full width at half magnitude (FWHM), $\Delta\omega$, of the transmission band of the defect mode when the incidence of the plane waves is normal (see curve *c* in Fig. 9). The parameters for curve *c* are the same as used in Sec. IV except for $S=5$. Curve *c* has a minimum value of $\Delta\omega_{\min}=3.8143\times10^{-4}\omega_0$, when $n_B=1.96$. In the case of the conventional PCs, it is obvious that one would prefer to the minimum point in curve *c* where the value of n_B is minimum. Dependence of $\Delta\omega$ on the structure parameters is another factor that we should consider in designing a practical omnidirectional filter.

The efforts as follows are focused on calculating the dependence of the optimized structural parameters (OSP) and maximum zero-dispersion angle (MZDA) upon n_B, which may provide the optimized parameters for omnidirectional filters. For this purpose, we pursue different criteria for zero dispersion.

The first criterion for zero dispersion relates to the definition of a fixed frequency range, $\omega_0\pm\Delta\omega$, which is the most conservative frequency range to guarantee zero dispersion. According to this criterion, any defect mode with a transmission peak in the frequency range of $\omega_0\pm\Delta\omega$ would be regarded as one that has a frequency of ω_0. Let $\Delta\omega$ be equal to the half of the minimum FWHM (i.e., $\frac{1}{2}\Delta\omega_{\min}$, the half of the minimum value of curve *c* in Fig. 9), we can calculate the OSP and MZDA, as shown in Fig. 10 in which curves *a* and *b* represent the OSP for TE and TM modes, respectively, while curves TE and TM denoting the MZDA for TE and TM modes, respectively. Curve *c* in Fig. 10 is equivalent to curve *a* in Fig. 9, which is calculated according to Eq. (6) and is depicted here for comparison. One can see from Fig. 10 that large angular filters can be realized when the value of n_B is large enough, but neither TE mode nor TM mode is omnidirectional.

We can also consider a varying frequency range to define the criterion for zero dispersion. This still means that any mode with a transmission peak in the frequency range of $\omega_0\pm\Delta\omega/2$ is regarded as one that has a frequency of ω_0. But now the value of $\Delta\omega$ varies with the structural parameters. We can choose one of the values, $\Delta\omega(n_B)$ for example, according to curve *c* in Fig. 9, and then calculate the OSP and MZDA. In Fig. 11 are shown the calculation results. As shown in Fig. 11, omnidirectional filter for TE mode can be realized when the value of n_B is larger than 3, but TM mode is not omnidirectional.

It is known that the insert loss of any optical device in optical communication system must be less than 2 dB. For optical filters, this means that the transmission must be more than 95%. Therefore, we can regard any mode as one that has a frequency of ω_0, if its transmission at frequency ω_0 is more than 95%. According to this criterion, the OSP and MZDA are calculated and shown in Fig. 12. We can see that omnidirectional filter for TE mode can be realized when the value of n_B is larger than 3.75, and that TM mode is still not omnidirectional.

Comparing the results shown in Figs. 10–12, one can find that the MZDA and OSP for different criterion are not the same, but that their changing trends with n_B are similar. The first trend is that the MZDA for TE mode increases when the value of n_B increases. The situation of TM mode is almost similar to that of TE mode, except that the MZDA for TM mode decreases when the value of n_B is close to the value of n_A. This decrease can be explained as follows. Increasing the value of n_B would decrease the width of the forbidden gap and finally destroy the condition for omnidirectional reflection. As the condition for omnidirectional reflection is being destroyed, the MZDA decreases rapidly. According to Fig. 1, one can see that the width of the forbidden gap for TE mode

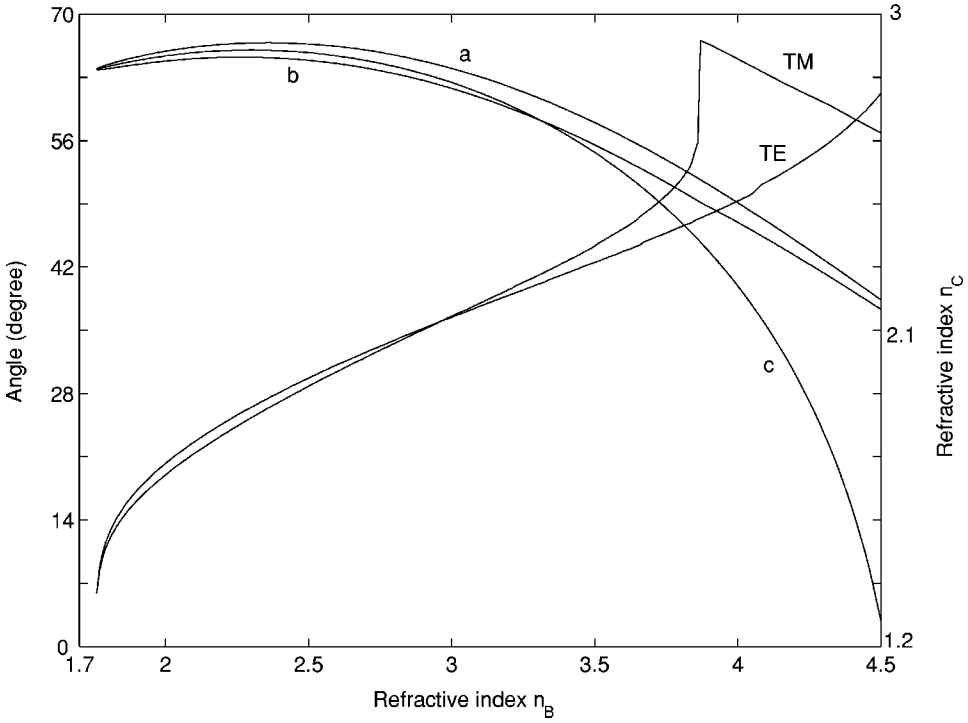

FIG. 10. Dependence of the optimized structural parameters (curve *a* for TE mode and curve *b* for TM mode) and maximum zero-dispersion angles (curve TE for TE mode and curve TM for TM mode) upon n_B according to the first criterion for zero dispersion.

with a large K is much larger than that of TM mode. This means that the condition of omnidirectional reflection for TE mode is more difficult to violate.

In addition, one can also see in Figs. 10–12 that curve *c* is always in the middle of curves *a* and *b* at a low value of n_B. This implies that the structural parameters derived from Eq. (6) can be used as initially tentative parameters in the optimal design of omnidirectional filters. When the value of n_B increases enough, the limit of $n_r^S > 15$ will finally be violated, and curve *c* will gradually leave curves *a* and *b*, as shown in Figs. 10–12.

VI. SUMMARY AND CONCLUSIONS

In summary, we demonstrate that the defect modes in 1D PCs containing a defect layer with a negative refractive index possess some additional properties in contrast with that in the conventional PCs. These properties include dispersion multiplicity, weak frequency dependence, and simultaneous emergence and splitting transition of multiple degenerate defect modes. Although the dispersion of the negative refractive index layer has been ignored in our study, one can expect that all of these unique properties of the defect modes

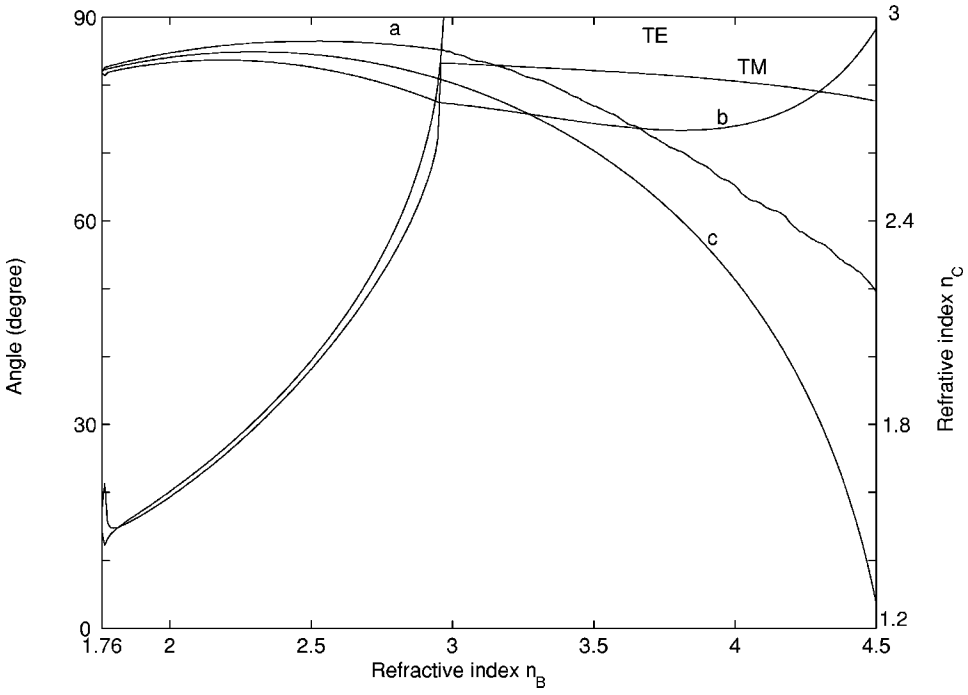

FIG. 11. Dependence of the optimized structural parameters (curve *a* for TE mode and curve *b* for TM mode) and maximum zero-dispersion angles (curve TE for TE mode and curve TM for TM mode) upon n_B according to the second criterion for zero dispersion.

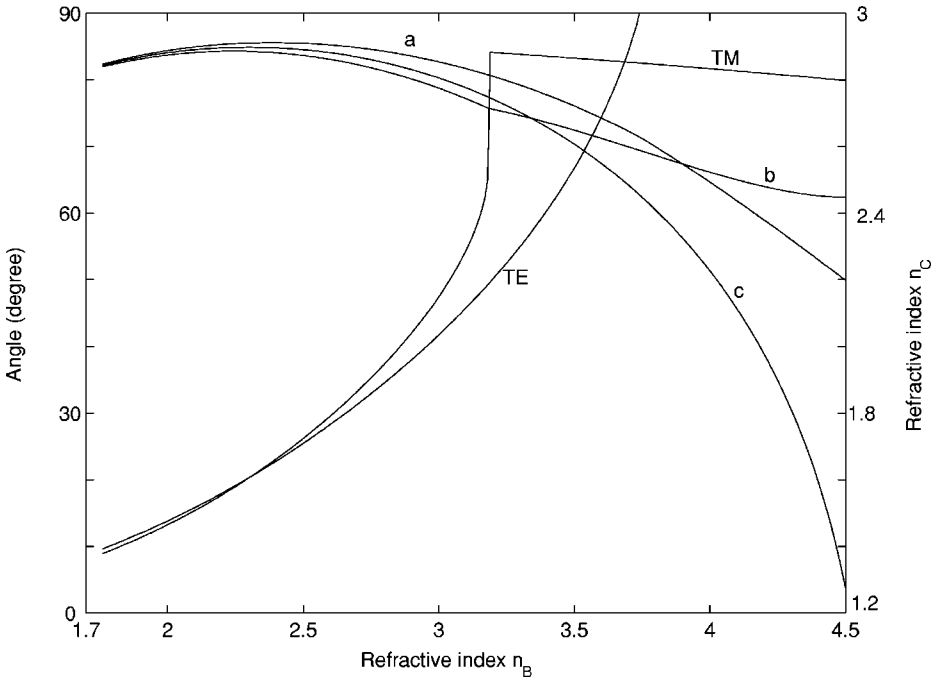

FIG. 12. Dependence of the optimized structural parameters (curve *a* for TE mode and curve *b* for TM mode) and maximum zero-dispersion angles (curve TE for TE mode and curve TM for TM mode) upon n_B according to the third criterion for zero dispersion.

still exist when the dispersion of the negative refractive index media is considered. All these unique properties are the results of the competition between Bragg effect and the physical properties of the defect layer with a negative refractive index, and can be understood by the two approximate formulas, Eqs. (6) and (8), respectively derived in Secs. III and IV. These unique properties prove to be useful in designing novel filters.

Based on the zero-dispersion phenomenon, a practical design for large incident angle filters with no polarization effect is proposed. A combined structure of two 1D defective PCs, in which one is designed to be of negative dispersion and the other of positive dispersion, is found to be a prototype of narrow frequency and sharp angular filters. In addition, the properties of week frequency dependence and simultaneous emergence of multiple defect modes can be used to design novel filters with a rectangular profile and multiple channeled filters. Optimal design of omnidirectional filters is also discussed in details. Based on three types of criteria proposed for zero dispersion, the optimized parameters for the omnidirectional filters are calculated.

The distributions of the electromagnetic fields in 1D PCs containing a defect layer with a negative refractive index are also calculated.

ACKNOWLEDGMENTS

This work is supported in part by National Basic Research Program of China (under Sub-Project 2004CB719804).

[1] E. Yablonovitch, Phys. Rev. Lett. **58**, 2059 (1987).
[2] S. John, Phys. Rev. Lett. **58**, 2486 (1987).
[3] Y. Fink, J. N. Winn, S. Fan, C. Chen, J. Michel, J. D. Joannopoulos, and E. L. Thomas, Science **82**, 1679 (1998).
[4] S. D. Hart, G. R. Maskaly, B. Temelkuran, P. H. Prideaux, J. D. Joannopoulos, and Y. Fink, Science **296**, 510 (2002).
[5] J. Li, L. Zhou, C. T. Chan, and P. Sheng, Phys. Rev. Lett. **90**, 083901 (2003).
[6] H. Jiang, H. Chen, H. Li, and Y. Zhang, Appl. Phys. Lett. **83**, 5386 (2003).
[7] J. Pendry, Nature (London) **423**, 22 (2003) and references therein.
[8] P. V. Parimi, W. T. Lu, P. Vodo, and S. Sridhar, Nature (London) **426**, 404 (2003).
[9] J. Gerardin and A. Lakhtakia, Microwave Opt. Technol. Lett. **34**, 409 (2002).
[10] Liang Wu, Sailing He, and Long Chen, Opt. Express **11**, 1283 (2003).
[11] H. A. Macleod, *Thin-film Optical Filters*, 2nd ed. (Adam Hilger Ltd., Bristol, 1986).
[12] G. Liang, P. Han, and H. Wang, Opt. Lett. **29**, 192 (2004).
[13] K. Sokada, *Optical Properties of Photonic Crystals* (Springer-Verlag, Berlin, 2001).
[14] S. D. Smith, J. Opt. Soc. Am. **48**, 43 (1958).
[15] C. R. Pidgeon and S. D. Smith, J. Opt. Soc. Am. **54**, 1459 (1964).
[16] Z. Wang, L. Wang, Y. Wu, L. Chen, X. Chen, and W. Lu, Appl. Phys. Lett. **84**, 1629 (2004).
[17] M. Scalora, J. P. Dowling, C. M. Bowden, and M. J. Bloemer, Phys. Rev. Lett. **73**, 1368 (1994).
[18] P. Yeh, *Optical Waves in Layered Media* (John Wiley & Sons, New York, 1988).
[19] Z. M. Zhang and C. J. Fu, Appl. Phys. Lett. **80**, 1097 (2002).
[20] M. N. Cherepanova and N. S. Makarina, Sov. J. Opt. Technol.

46, 57 (1979).
[21] H. Lee, H. Makino, T. Yao, and A. Tanaka, Appl. Phys. Lett. **81**, 4502 (2002).
[22] P. Baumeister, Appl. Opt. **31**, 504 (1992).
[23] D. Cushing, in *Optical Interference Coating*, Vol. 9 of 1998 OSA Technical Digest Series (Optical Society of America, Washington, DC, 1998), pp. 226.
[24] P. Gu, H. Chen, Y. Zhang, H. Li, and X. Liu, Appl. Opt. **43**, 2066 (2004).